Engineering Structures 327 (2025) 119627

Contents lists available at ScienceDirect

Engineering Structures

journal homepage: www.elsevier.com/locate/engstruct

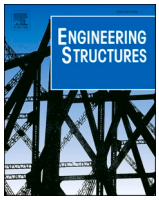

Damping assessment of monopole steel structures through full-scale experiments

Luisa Pagnini *, Andrea Orlando, Maria Pia Repetto

Department of Civil, Chemical and Environmental Engineering (DICCA), University of Genoa, Genoa, Italy

A B S T R A C T

This paper investigates the modal damping ratios of steel monopole structures, with a focus on their relevance in structural design. Full-scale dynamic identification tests were conducted on three distinct monopoles to reveal damping values in relation with wind speed and motion amplitude. Additional data from the literature on similar structural typologies are incorporated providing information on the testing methodologies and motion amplitude. Finally, the data are categorized to identify primary trends across monopole structures, supplying information on damping ratios useful for structural dynamic response calculations. Particular attention is given to the damping ratio of the second vibration mode, focusing on a specific case where it is significantly lower than that of the fundamental mode. In such cases, regulatory standards may lead to overestimations of structural damping, potentially resulting in non-conservative design assessments.

1. Introduction

Steel monopole cantilevers are employed across a diverse range of structures, including but not limited to lighting poles, telecom towers, chimneys, traffic signals, wind turbines, and lightning rods. Due to their slenderness and lightweight design, these structures are particularly susceptible to gust actions and aeroelastic effects. Gust actions mainly involve the first vibration mode, resulting in alongwind and crosswind vibrations (e.g., [12]). However, the contribution of the second mode can also be significant in very tall and slender structures [75]. Another excitation mechanism is given by aeroelastic phenomena. Among these, galloping may arise at the presence of aerodynamically unstable shapes that differ from the circular ones (e.g., [62]). Vortex-Induced Vibrations (VIVs) are key design conditions for these types of structures (e.g., [26, 56]) and are primarily influenced by the Strouhal number and a mass-damping parameter, such as the Scruton number [46,49]. The Strouhal number dictates the frequency at which vortices are shed from the structure, thereby determining the critical velocity during resonance. The Scruton number is directly ruled by the structural damping and controls the range of synchronization during lock-in conditions and the vibration amplitude [68,69].

VIVs commonly occur at moderate and frequent wind velocities in resonance with the first vibration mode. While VIVs on higher modes have also been observed [2] and are occasionally documented on technical web sites through videos, they are rarely reported in scientific papers [13], and are mainly limited to wind tunnel tests [26,72]. The specific design and shape of high-mast supports can amplify the risk of structural issues. Repetto and Solari [56] investigated vortex-induced vibrations in a lightly damped antenna tower encased in a fiberglass cylinder. The study found that the casing at the top reduced the Scruton number, leading to lock-in conditions. Severe vibrations might also concern very slender, unadorned columns, as in the case of lightning rods, where the absence of ancillaries prevents energy dissipation due to friction in joints or other contributions beyond those of the column itself with its foundation, making the damping extraordinarily low and eliminating any disturbance to regular vortex shedding [21]. Consequently, resonant wind speed may result small enough for being characterized by frequent occurrence and, in the meanwhile, large enough to induce significant structural vibrations and repeated stress cycles [54-56]. Pole collapses due to strong winds usually occur near the base, often in sections weakened by inspection openings. Das et al. [18] examined the failure of a light mast that bent at the maintenance pocket during a high-speed storm. Chen et al. [15] report widespread failure of light poles on an elevated highway bridge that were exposed to a hurricane in Louisiana. Frequent cracks in the weld area at the base of the column, anchor rods and swage joints often emphasize fatigue damage as the primary cause of collapse for chimneys [67], high-mast light towers [3,73], highway light poles [12,66,76], wind turbine towers [37] and lightning rods [74], leading to serious consequences for site functionality and the integrity of hosting infrastructure. Structures with similar characteristics are often installed in large numbers at a single site. Examples include roadside lighting poles and traffic signals, wind turbines in wind farms, and lightning rods at industrial facilities. If one of these structures fails or collapses, it typically triggers a

* Corresponding author.
E-mail addresses: luisa.pagnini@unige.it (L. Pagnini), andrea.orlando@edu.unige.it (A. Orlando), maria.pia.repetto@unige.it (M.P. Repetto).

https://doi.org/10.1016/j.engstruct.2025.119627
Received 1 September 2024; Received in revised form 24 November 2024; Accepted 2 January 2025

comprehensive inspection of all similar installations to ensure safety and prevent further incidents. These assessments may reveal fatigue cracks or other issues, warranting the dismantling of the entire array of structures [17].

Wind codes and standards [16,22] outline calculation procedures for gust actions and VIVs, providing structural damping values for a broadly defined category of structures. Other documents [1] specifically address tubular towers, highlighting the significant concern regarding fatigue cracking of column and base details in lightly damped structures. NCHRP [19] points out the importance of considering vortex shedding resonant with higher modes supplying practical examples. However, significant challenges remain in estimating this parameter, as errors can lead to large variations in wind effect predictions [39,40,47]. This poses a critical issue in safety engineering assessment, influencing both the design process and subsequent interventions, such as the implementation of dampers. If the damping values proposed by the standards and codes are deemed inappropriate, these documents explicitly suggest conducting tests on existing structures to obtain reliable estimates [23].

Field tests for dynamic identification are especially beneficial with structures that have exhibited potential issues, as they support structural verifications and design interventions. The scientific literature documents several in-field measurements on steel monotubular towers that were conducted after signs of fatigue failure were observed. An extensive inspection of high-mast towers in Iowa [17] and Wyoming [2] revealed fatigue cracks on many structures and loose anchor bolts on many others. Full scale measurements were then carried out for the dynamic identification of similar towers. Following the failure of a huge number of aluminum light poles, field tests were carried out by Caracoglia and Jones [12] to investigate fatigue phenomena induced by VIVs, and by Zuo and Letchford [76] to investigate buffeting induced vibrations. Siringoringo et al. [60] carried out measurements on light poles on elevated highway bridges that had exhibited large vibration amplitudes.

To prevent damage scenarios, other tests were carried out to provide designers with suitable values of damping ratios. Pagnini and Solari [48] investigated prototypes of three different typologies of interest for Italian manufacturers: a high-mast light tower designed to illuminate squares and service areas, two lighting poles for streets and highways, and a decorative column for urban lighting. Jimenez Capilla et al. [29] investigated telecommunication structures to enhance the design of steel poles used for similar applications. Further tests have been conducted on individual structures (e.g., [44,71]).

Although the investigations mentioned above provide a broad range of case studies identified by modal damping, there is limited effort to synthesize these results through a consistent approach for a comprehensive analysis of the data. Analyzing the data as a whole remains challenging due to inconsistencies in test conditions, which often vary in structural displacement levels and measurement accuracy. Additionally, the characterization of higher vibration modes is still rare.

The GS – WinDyn research group at the University of Genova has undertaken an extensive research project on structural monitoring and wind measurements. The primary aim of this activity is to investigate wind-excited response models of slender structures [41,43], analysing the role of dynamic parameters under both synoptic and non-synoptic winds [34]. The structures analysed are mainly located in port areas, where a wind monitoring network was established as part of the European Project “Wind and Ports” [63] and “Wind, Ports, and Sea” [10]. This network was further developed under the THUNDERR project [61], which specifically focused on analysing non-stationary events. As part of this effort, the project included a monitoring system on a lattice tower in Romania [11], two small size wind turbines that had been monitored for about 5 years [42,45], a reinforced concrete bridge monitored for one year [38] and ongoing measurements on two lighting towers. The monitoring program was recently expanded to include full-scale measurements on a lightning rod to determine its damping for assessing fatigue resistance [70].

To address the lack of a unified discussion of structural damping data in the literature, this paper analyzes measured values for various typologies of steel monopoles based on homogeneous typological classes, and represents these values in relation to the deformation state and wind speed. After briefly reviewing the dynamic identification techniques used in this study (Section 2), the paper describes the dynamic identification of a slender lightning rod made of a bare tubular cantilever (Section 3), a medium-height light pole equipped with a ladder and platforms (Section 4) and a high-mast light tower (Section 5). Section 6 incorporates additional data from other monopole structures sourced from technical reports and scientific literature, gathering and selecting datasets that provide pertinent details, along with the wind speed or motion amplitude associated with the estimates of damping. In Section 7 the collected data are categorized and discussed to identify the main trends in damping ratios based on the specific characteristics of these structures, drawing some conclusions on the estimation of damping in structural calculations (Section 8).

2. Notes on structural identification techniques

Several criteria exist for the experimental identification of damping either based on forced or ambient vibration measurements (e.g., [24,31,65]). Referring to the extensive scientific literature regarding the various techniques of modal identification (e.g., [5,53]), this section focuses on the methods used in the research.

Experimental Modal Analysis (EMA) consists of classical modal testing methods based on the response measurements from controlled force, including also impulse loads or imposed displacements [8]. The forced vibration test enables controlled and repeatable excitations, yielding clear responses that minimize noise and ambiguity. The tubular column is a prototype to which one can quite easily impose a static deformation followed by a sudden release that induces decaying oscillations in time t. The free response x consists of a sum of damped sinusoidal waves [30]:

$$x(t) = \sum_i x_{oi}\, e^{-2\pi n_i \xi_i \tau} \left(\cos \sqrt{1-\xi_i^2}\; 2\pi n_i t + \gamma_i \right) \tag{1}$$

where n_i and ξ_i ($\xi_i \ll 1$) are the fundamental frequency and damping ratio of mode i-th, x_{0i} and γ_i are the amplitude and phase determined by the initial conditions. The damped wave components can be separated using band-pass filtering. Then, n_i is easily readable from the harmonic part, while ξ_i is directly obtained by fitting the oscillation decay envelope. This approach reduces reliance on assumptions or pre-set model parameters, which are typically required in ambient vibration methods.

Unfortunately, the implementation of free vibration tests is often unfeasible for the needed logistic, while ambient vibration tests have the significant advantage of being practical and economical. In such cases, alternative avenues are explored, utilizing the response recording of the structure during its typical usage. The class of Operational Modal Analysis (OMA) techniques provides the dynamic identification from ambient response, under the assumption that excitation is random and stationary. In last decades, OMA has been systematized with new effective output-only modal identification procedures that overcome limitations related to closely spaced modes, noise and excitation having some spectral distribution [8]. Nowadays, OMA is a widely applied tool (e.g., [57]) with several successful applications in civil [14,35,59] and mechanical engineering [6,52] also developed with automated procedures [20].

Investigations carried out in this paper employ two distinct OMA methods to identify modal frequencies and damping ratios under ambient excitation, namely, the Enhanced Frequency-Domain Decomposition (EFDD), operating in the frequency domain, and the Data-Driven – Stochastic Subspace Identification (SSI-data), which operates in the time domain.

Relying on white noise excitation, at least in the neighbourhood of

the investigated frequencies, the EFDD [27,31,9] estimates frequencies and damping ratios by line-fitting the first eigenvalue (or singular value) of the Power Spectral Density (PSD) matrix of the measured response in the frequency domain, n. In the neighborhood of each resonance frequency, the response is approximated by the square modulus of the frequency response function of a single DoF system:

$$SV(n) = \frac{SV_i}{\sqrt{\left(1-\frac{n^2}{n_i^2}\right)^2 + 4\xi_i^2\frac{n^2}{n_i^2}}} \tag{2}$$

where n_i, ξ_i and SV_i are to be determined through least squares fitting, also providing an estimate of the frequency and peak value that best approximate the experimental response [45]. Besides ensuring a user-friendly and efficient processing procedure, as well as providing physical evidence, the quality of the results is closely linked to the careful selection of parameters for spectrum computation. Moreover, damping estimation may lose accuracy when modes are closely spaced.

Given the basic conditions of linearity, stationarity and response observability, SSI [50,51] considers the measured response as the output of the mechanical system under investigation excited by unknown forces that are the output of a so-called excitation system, loaded, in turns, by a Gaussian white noise. In this way, the measured response is interpreted as the output of a combined system, made by the excitation system and the structure under test in series. The SSI-data algorithm projects the row space of the future outputs into the row space of the past reference outputs, instead of all past outputs, reducing the dimension of the matrices and the computation time. The separation of the physical poles from the spurious mathematical ones takes advantage of the so-called stabilization diagram, showing the poles obtained for different model orders as a function of the corresponding frequency. By tracking their evolution, alignment of stable poles identifies the physical modes, while the spurious mathematical ones tend to be more scattered and typically do not stabilize. Besides offering highly accurate parameter estimation and computational efficiency compared to other OMA methods, SSI is a mathematically complex approach. Careful interpretation and validation are essential to ensure that the identified poles correspond to the true physical dynamics of the system.

Even with reliable data, the inherent random nature of damping means that results will never be exactly the same across different techniques due to the varying assumptions of each method (e.g., [31]). Additionally, the choice of parameters (e.g., frequency resolution in EFDD, model order in SSI) can further increase the variability. These uncertainties become more pronounced for low damped structures [7] and when data quality is medium to low. Consequently, gathering consistent results from diverse sources can be challenging. In recent years, dynamic identification methods have increasingly focused on advanced Bayesian techniques [5], such as the Bayesian Fast Fourier Transform [4], which offer probabilistic insights into system parameters and improve robustness by rigorously accounting for uncertainties in the identification process.

3. Field test on a lightning rod

In recent times, some lightning rods within an industrial site have encountered structural problems that were attributed to fatigue damage. The fatigue life assessment for the entire array of rods revealed potential fatigue issues in both the first and second modes, depending on the value of structural damping used in the calculations [70]. For this reason, given the well-known uncertainties in estimating this parameter, an experimental campaign has been undertaken to characterize an uncracked tower prototype through on-site dynamic identification tests.

3.1. Description and test set up

The analyzed lightning rod is a 30 m conical pole made of three sections joined with telescoping lap joints. It has 16-sided polygonal sections with outer diameter 0.77 m at the base, 0.24 m at the top, and thickness 4 mm. It is free of any appendages or ancillaries along its height.

The dynamic identification test was conducted over a single day. The structure was monitored by 2 Lunitek Sentinel-M accelerographs which integrate Wi-Fi triaxial mems accelerometers with a 20 bit resolution and a self-noise level of less than 18 μg/$\sqrt{}$Hz. An integrated memory bank allows to manage a ring-buffer for long continuous recordings. Data are sampled at 500 Hz. The internal GNSS receiver allows to synchronize the two sensors with the absolute time. One sensor is positioned at the top level, z = 30 m, where the contributions of the first two modal shapes are most pronounced. Based on the outcomes of a finite element model (FEM) of the structure (see [70]), the second sensor is positioned at the height z = 16 m, corresponding to the anti-node of the second mode. Each one acquires along two horizontal directions denoted by x, y; the vertical component is not considered.

First, the ambient response was recorded for about 2 hours. Anemometric surveys recorded minimal wind activity, with wind speeds ranging from 1 to 2 m/s. Free decaying vibrations were induced by the sudden release of a tensioned cable, attached to a collar at the column's top and pulled from the ground using a winch. To avoid interference with structural oscillations, the cable was released at the top of the pole via a steel bar, designed through FEM analysis to break under a specific force. To minimize transverse deformation, the bar was encased in a metal cylinder terminating in two rings for connection to the collar and the cable. Set at an angle of approximately 30 degrees to the horizontal plane, the cable was tensioned with a force of about 1.3 kN, resulting in a horizontal component of 1.1 kN, and a horizontal top displacement of 15 cm. Fig. 1 depicts some key moments of the tests: the live cable (Fig. 1a), the specimen for the release and the metal bar broken after the test (Fig. 1b), the released cable (Fig. 1c).

3.2. Ambient vibrations

Fig. 2a shows the time history of the two horizontal acceleration components α=x, y of the ambient vibrations recorded by the sensors. Standard deviation $\sigma_{\ddot{\alpha}}$ and peak values $\ddot{\alpha}_{max}$ of the accelerations at $z = 30$ m are: $\sigma_{\ddot{x}}$= 0.21 m/s^2, $\sigma_{\ddot{y}}$= 0.17 m/s^2; $\ddot{x}_{max}$= 1.27 m/s^2, $\ddot{y}_{max}$= 1.22 m/s^2.

Fig. 2b shows the PSD functions. Fundamental frequencies are n_1= 0.87 Hz; n_2= 3.60 Hz; n_3= 8.72 Hz.

Vibration amplitudes are quite small, since wind speed was very low during the experiments. Damping identification is carried out by EFDD, implemented a MATLAB code [32] and SSI-data/ref, implemented with the commercial tool Macec [58] and the Signal Processing Toolbox of Matlab. SSI-data/ref shows pairs of stable poles at very close, nearly coincident frequencies characterized by different damping values that are associated to directions x and y.

Table 1 reports damping ratios in the x and y directions revealing small variations between different testing methods. Estimates uniformly indicate a low dissipative capacity in the first vibration mode, and extremely low on the second mode. The scattering in the third mode values highlights that its contribution is quite small for being properly appreciated.

Given the very low excitation level, results from ambient vibration measurements serve as valuable preliminary data for forced vibration tests by providing an initial estimate of natural frequencies and damping ratios to be determined.

3.3. Results from pull and release tests

Three pull-and-release tests were conducted sequentially, imposing the top displacement in the y direction. Fig. 3a shows the free decay of acceleration at top recorded during one of these tests, Fig. 3b shows its

Fig. 1. Live cable (a), specimen for the release and the metal bar broken after the test (b); released cable (c).

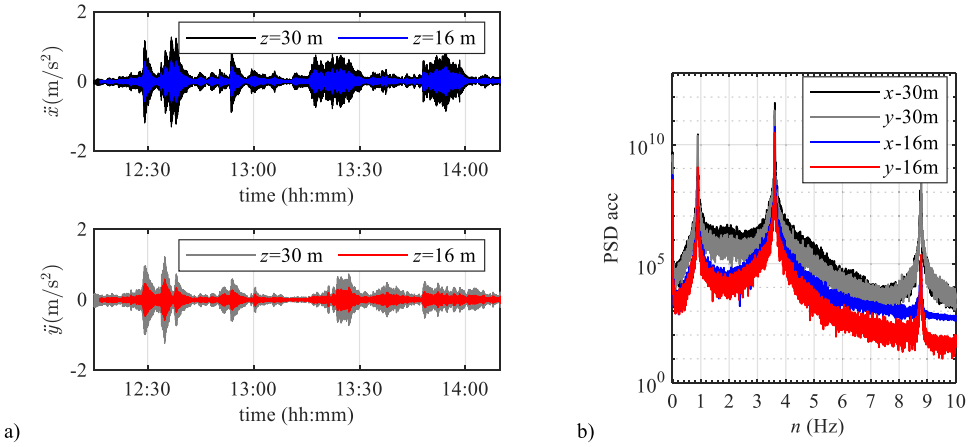

Fig. 2. Time history (a) and PSD (b) of the ambient vibrations.

Table 1
Modal damping ratios from ambient vibrations.

OMA technique	ξ_{1x}, ξ_{1y} (%)	ξ_{2x}, ξ_{2y} (%)	ξ_{3x}, ξ_{3y} (%)
EFDD	0.31, 0.17	0.02, 0.03	0.10, 0.06
SSI-data/ref	0.29, 0.15	0.02, 0.02	0.06, 0.04

PSD. The application of a suitable band-pass filter helps in eliminating possible contributions from other modes, allowing for a focus solely on the mode under investigation. Assuming displacement as a representative parameter of the deformation state [48,76], Fig. 4a and Fig. 4b show the free decay of displacement corresponding to the first and second vibration modes, respectively. This is approximately obtained by dividing the filtered acceleration signal for the *i*-th vibration mode by

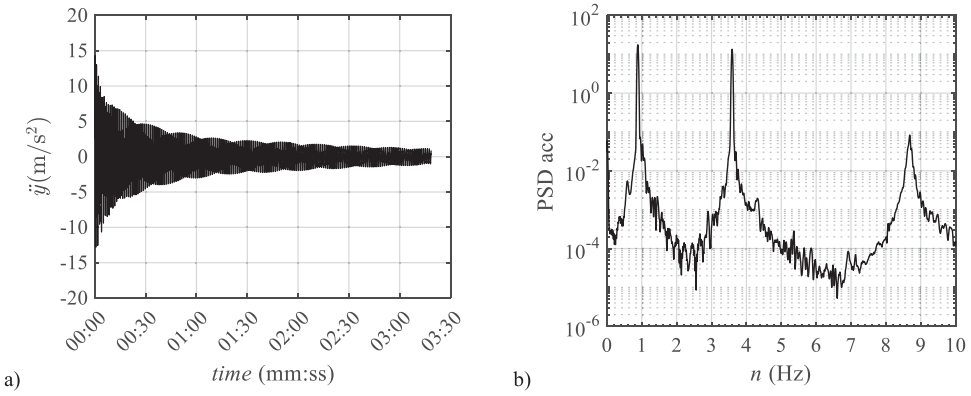

Fig. 3. Test n.2, measurement at top: free acceleration decay (a); its PSD (b).

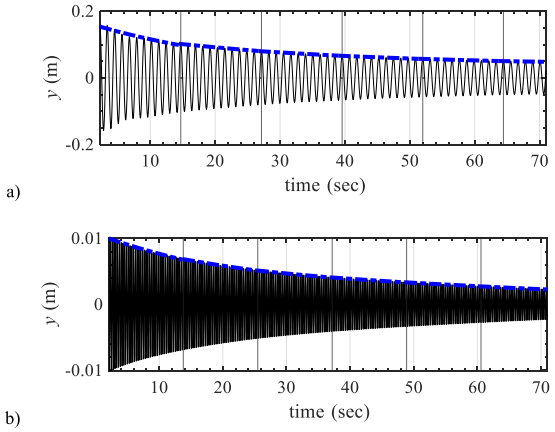

Fig. 4. Test n.2. Free displacement decay of the first (a), second (b) mode component.

$(2\pi n_i)^2$. The dashed blue line represents the logarithmic decay of the peak envelope that is segmented into multiple windows (delimited by the vertical lines in the diagram). For each window, damping ratio is estimated versus the average vibration amplitude.

Fig. 5a, b shows the results obtained for the first and second vibration mode versus the displacement at the top d for the selected mode. Different symbols indicate results derived in the different test cases; black solid and void symbols show values obtained from the sensor at top, $z = 30$ m, and at $z = 16$ m, respectively. The grey stripe reported in the diagrams represents the range of values obtained from the ambient vibration test.

For the first mode of vibration (Fig. 5a), at low displacements, up to about $d = 50$ mm, the damping estimates in test number 3 exhibit values higher than those observed in other tests, therefore, it is deemed appropriate to exclude them from subsequent evaluations. The values obtained from the other tests (still for d<50 mm) are stable at $\xi_1 = 0.17$ %. However, they increase with the motion amplitude, exceeding 0.35 % at $d = 100$ mm. Damping ratios for the second mode (Fig. 5b) are quite low, increasing from $\xi_2 = 0.06$ % to $\xi_2 = 0.15$ %. Damping ratio estimates for the third mode lack sufficient reliability due to the absence of a clear logarithmic decrease in the structural response.

The results from the ambient test closely align with the estimates from the free response decay for the first vibration mode at small displacement levels, while they are even smaller for the second mode. In this case, the minimal amplitude of the environmental response further reduces the damping, while also increasing the uncertainty of the estimate. Given the substantial uncertainties associated with structural damping and its estimation, the results from the test campaign offer a consistent overview, indicating extremely low values for all the analyzed modes.

4. Field tests on lighting tower with ladder and platforms in La Spezia

In the harbour of La Spezia, we are assessing a 16.6 m conical column (Fig. 6) with a 16-sided polygonal cross-section, consisting of two sections overlapped by a telescoping joint. Its outer diameter starts at

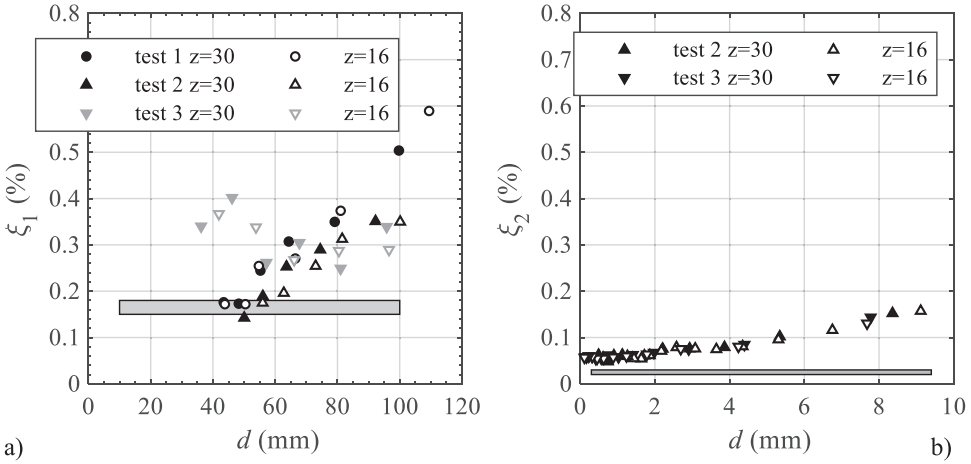

Fig. 5. Damping ratio for the first (a), second mode (b) versus displacement at the top; the measurement direction coincides with y axis. Grey stripes report results from ambient vibration test.

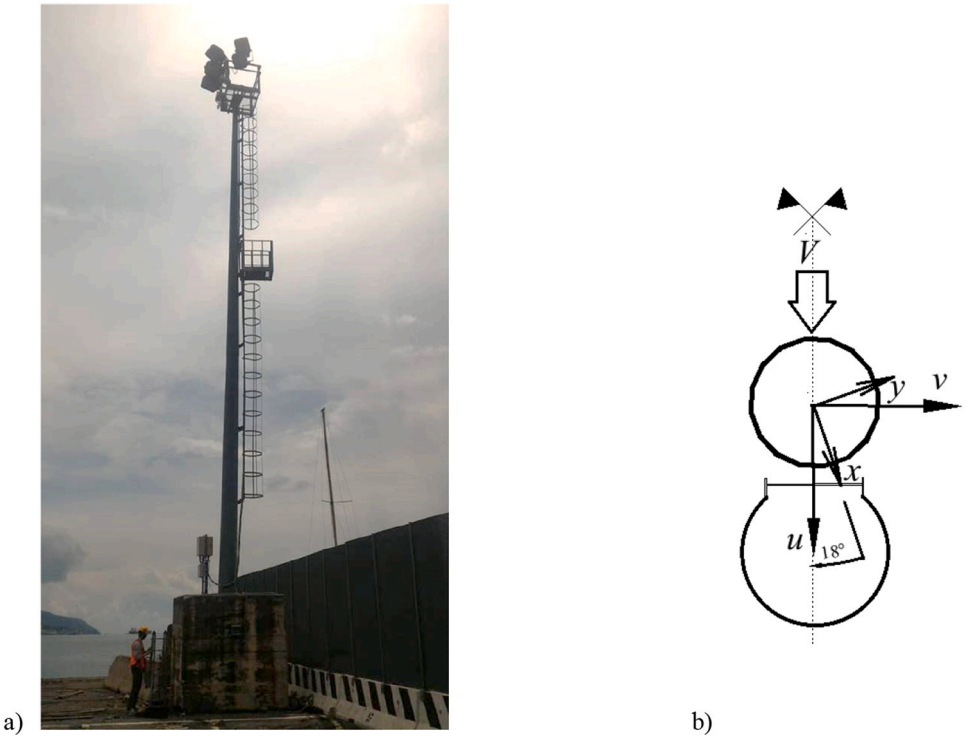

Fig. 6. Lighting pole in La Spezia (a), drawing and position of the sensors (b), cross section and recording directions c).

0.53 m at the base, tapering to 0.25 m at the top, with a thickness of 5 mm. A sturdy steel ladder ascends along its height, providing access to a platform at the top, which houses units for lighting and other equipment, as well as a resting platform. More details can be found in Mengistu et al. [33].

A three-axial ultrasonic anemometer, mounted on the upper platform, records the three components of wind speed at a sampling frequency of 10 Hz. Two biaxial MEMS accelerometers (Dytran 7533A1, self-noise $< 250\ \mu g/\sqrt{Hz}$) record the structural horizontal acceleration, one at the top of the pole, and the other at 10.5 m above the ground, corresponding to the anti-node of the second bending mode according the FEM model of the structure [36]. The data acquisition unit is the System 8000 by Micro-Measurements, which communicates with a host mini PC via Ethernet and transfers data to headquarters through a cloud-based connection. Accelerations are sampled at 200 Hz. Fig. 6b shows a cross section of the pole with the ladder where the recording directions (x, y) form an angle of 18° with the symmetry axes. The investigation is conducted using selected time histories where the direction of the mean wind speed (V) aligns with the symmetry axis of the pole and ladder ensemble, with the ladder positioned on the downwind side; u, v are, respectively, the alongwind and crosswind directions (see Fig. 6b). Eight mono-axial half-bridge strain gauges are placed at the bottom of the tower to investigate the static and quasi-static response of the structure. All sensors are cable-connected to a data acquisition system inside a watertight booth at the foot of the structure, also driving the real-time data transmission.

Fig. 7 reports the PSD of the structural acceleration at the top obtained from a selected 1-h ambient record at mean wind velocity 6 m/s. Fig. 7a presents the PSD of the acceleration records along the measurement axes, x, y, showing a variegated harmonic content related to the main structure and to secondary systems. In particular, the pair of frequencies n_{1A}= 0.74 Hz, n_{1B}= 0.84 Hz identifies fundamental modes along two orthogonal axes related to first modal shapes of the cantilever beam. The pair of frequencies n_{2A}= 3.62 Hz, n_{2B}= 3.93 Hz are representative of second modal shapes. Fig. 7b reports the alongwind (u) and crosswind (v) components, showing that n_{1A}, n_{2A} are modal frequencies of alongwind fundamental modes, while n_{1B}, n_{2B} are related to crosswind modes.

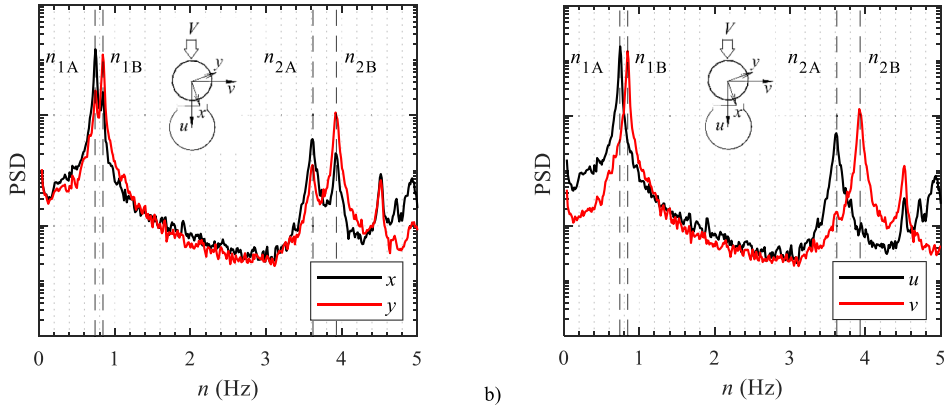

Fig. 7. PSD of acceleration at top of the lighting pole in La Spezia in the recording directions (a), in the alongwind and crosswind directions (b).

Fig. 8a, b show the first and second damping ratios obtained from 1 hour recordings selected for stationary wind speed. The first damping ratio increases rapidly with wind velocity due to the aerodynamic component. Structural damping can be derived from values at very low wind speeds ($V < 2$ m/s), and is quantified with an average value of $\xi_1 = 0.2$ %. The second damping ratio remains nearly constant around $\xi_2 = 0.7$ %, with no significant variation observed with wind velocity; $\xi_2 = 0.63$ % can be regarded as a prudential value supplying the first quartile. Both figures suggest that there are no substantial differences between alongwind and crosswind values.

5. Field tests on high-mast lighting tower in Genova

The lighting tower analyzed at Genoa Harbour stands 35 m tall and features a tapered structure made up of four segments, each consisting of 16-sided polygonal sections connected through telescoping joints (Fig. 9). The outer diameter at the base is 0.73 m, narrowing to 0.21 m at the top. The shaft thickness starts at 8 mm at the base and reduces to 5 mm at the top. It is free of any appendage and holds lighting equipment at top, with mass approximately 0.5 tonne.

Two biaxial piezo accelerometers (PCB piezotronics 3741F122G, self-noise $< 10\ \mu g/\sqrt{Hz}$) record the horizontal accelerations at 100 Hz, one at the top of the pole and the other at 23 m, to assess the contribution of the second bending mode. As in the previous case, 8 strain gauges are placed at the lower part of the tower. A three-axial ultrasonic anemometer is positioned at top. The data acquisition unit is the CompactRIO by National Instruments, which facilitates data transfer to headquarters via an FTP server.

The time histories analysed correspond to various mean wind directions. Fig. 9b shows the cross section of the pole, the measurement components x, y, the wind coming from a generic direction β. Due to the nearly polar-symmetrical configuration of the pole, the bending modes are expected to occur in pairs with almost identical natural frequencies [25]. Real-world conditions introduce some deviation due to the fact that the structure, which is located in an area frequented by heavy vehicles, has probably suffered some impacts. Fig. 10 reports the PSD of the alongwind (u) and crosswind (v) structural acceleration at top obtained from a selected 1-h ambient record (V=7 m/s), showing the modal frequencies $n_{1A} = 0.40$ Hz, $n_{1B} = 0.42$ Hz related to the first modal shapes of the cantilever beam, $n_{2A} = 1.94$ Hz, $n_{2B} = 1.98$ Hz that identify second-order fundamental modes. The contributions related to n_{1A}, n_{1B} arise in both the alongwind and crosswind components, with the contribution from n_{1B} being quite small in both u and v.

Fig. 11 shows damping measurements at different mean wind speeds and directions. The trend is qualitatively similar to that in Fig. 8. The first damping ratio increases rapidly with wind velocity. At low wind speeds ($V \approx 2$ m/s), the estimated structural component is quantified with an average value of $\xi_1 = 0.45$ %. Even in this case, no significant variation is observed on the damping ratio of the second mode with the wind speed, and the values stay around the average $\xi_2 \sim 0.3$ %, while $\xi_2 = 0.23$ % can be regarded as a prudential value supplying the first quartile.

6. Full-scale tests on steel monopoles retrieved from the literature

This section discusses the tests on lighting poles obtained by Pagnini and Solari [48], by other technical reports and scientific papers, and further tests conducted on other kind of monopole structures. Table 2 provides a detailed summary of the key information from the case studies. In the table, ξ_1 and ξ_2 are the average of the damping estimates at small wind velocities ($V \leq 2$ m/s) and structural displacements (indicatively, $d_1/H < 0.5$ %, $d_2/H < 0.02$ %, being d_1 and d_2 the maximum displacement associated to the first and second vibration mode)

6.1. Pagnini and Solari (2001) lighting pole tests

Pagnini and Solari [48] conducted pull and release tests on a high mast tower and two street lighting poles and derived damping ratios by the logarithmic decrement technique. The first structure, called Geo Tower, is a 30 m conical column (Fig. 12a) made of three superimposed twelve-sided polygonal sections. The lighting fixture at top has a diameter of 3.5 m and a mass of 800 kg, consists of two half-spheres, one of which is equipped with a lowering device for easier maintenance access. The second structure is 12 m high, with circular cross section made from a single sheet metal. The third is 10 m high (Fig. 12b), with circular cross section, constructed from five stepped shafts joined by circumferential welding nearby the steps. These two poles were tested both with and without a small lump at top, with results aligning conclusively. A fourth structure, shown in Fig. 12c, is a 14 m street furniture pole made of two octagonal superimposed shafts, supporting a 145 kg lighting fixture. In this case, a mechanical exciter was used to generate controlled vibrations resonant with the fundamental frequency using a rotating out of balance mass.

The measured damping ratios for the entire sample exhibit considerable variability both for the first and the second vibration mode. The values undergo a sudden increase with the vibration amplitude, exceeding $\xi_1 = 3$ % at $d \approx 0.7$ m for the Geo Tower, where the large lighting fixture contributes to higher energy dissipation. For these structures, Solari and Pagnini [62] assumed a structural damping ratio of 0.5 % for calculating gust actions and galloping conditions, 0.25 % for

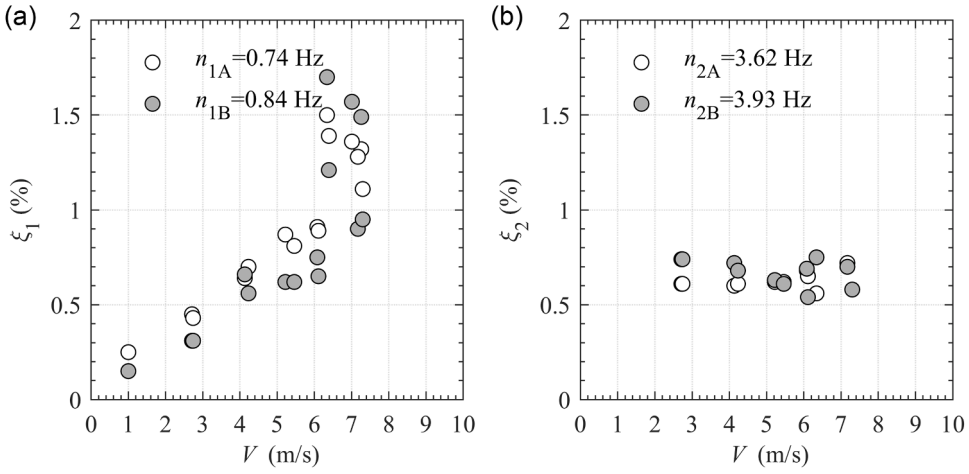

Fig. 8. First (a) and second (b) modal damping ratio versus mean wind speed of the lighting pole in La Spezia.

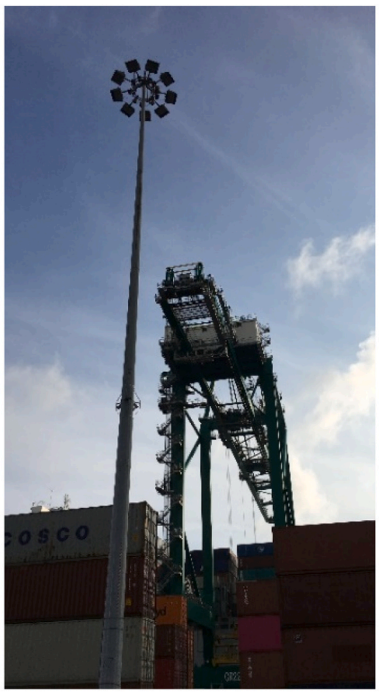

Fig. 9. Lighting pole in Genova (a), cross section and recording directions (c).

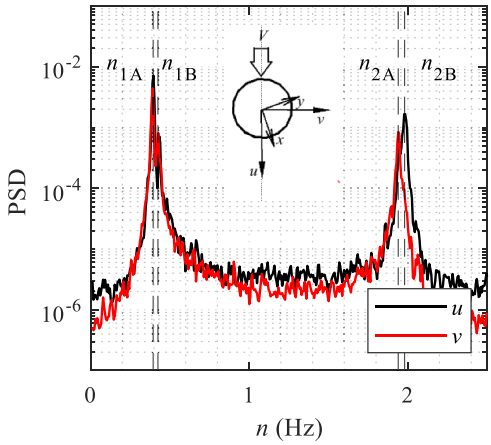

Fig. 10. PSD of acceleration at top of the lighting pole in Genova in alongwind and crosswind direction.

vortex induced effects.

6.2. Other tests on lighting poles

Caracoglia and Jones [12] reported measurements for a 13.7 m tapered straight aluminum-alloy pole with circular cross section (Fig. 13a) that was tested with and without the luminaire at top. Zuo and Letchford [76] performed a pull and release test on an aluminum light tower made by a 10.6 m tapering pole having circular section and a cantilever arm that extends outward by 3.6 m and rises by 1.7 m (Fig. 13b). Siringoringo et al. [60] conducted a dynamic identification of two 9.1 m viaduct poles, each with a lamp at the top and a signboard at mid-height (see Fig. 13c) estimating damping from low-level ambient vibrations using a video camera system.

Further dynamic identification tests conducted by Yam et al. [71], Connor and Hodgson [17], and Ahearn and Puckett [2] provide structural damping values of light poles but lack information on motion amplitudes or wind speed, both of which are highly significant factors. Consequently, these results are not included in Table 2. Nevertheless, they highlight damping ratios for the second vibration mode that are consistently lower than those for the first mode.

6.3. Other tests on monopole structures

Pagnini and Piccardo [44] investigated the ambient vibrations of a vertical axis wind turbine (VAWT) supported by a tapered 10.8 m steel monopole (Fig. 13d), made by two shafts with telescoping joint. The mass of the H-rotor is approximately 3 tonnes. This structure differs from the other monopoles in this research due to its larger cross-sectional dimensions and stiffness. However, the presence of a large mass at the top results in fundamental frequency similar to that of slender light poles. It also stands out due to its very low damping under calm wind and parked conditions, although increasing with wind speed and in rotation.

Jimenez Capilla et al. [28] recorded the structural response of a 14.5 m telecom monopole with mobile antennas at top (Fig. 13e), ladders, internal and external feeder cabling, exposed to wind gusts and high turbulence. The correlation between modal damping, as estimated by long-term monitoring measurements, and wind speed exhibits significant variability. From pull and release tests, Jimenez Capilla et al. [29] supply damping ratios and structural accelerations at top. Subsequently, the authors conducted pull-and-release tests on a large group of tapered telecom monopoles ranging in height from 14.5 m to 18 m. Estimates for ξ_1 and ξ_2 exhibit significant variability among structures of similar types, with damping ratios generally lower in the second mode. The authors do not provide the amplitude of motion.

7. Discussion

Fig. 14 and Fig. 15 presents the ensemble of estimates for the first and second modal damping ratio of the collected structures. The data are grouped into poles with ancillary components, such as ladders, large luminaires, or other equipment, indicated in black in the following figures, and poles without ancillary components, indicated in blue. Building on the original values, specific adjustments have been

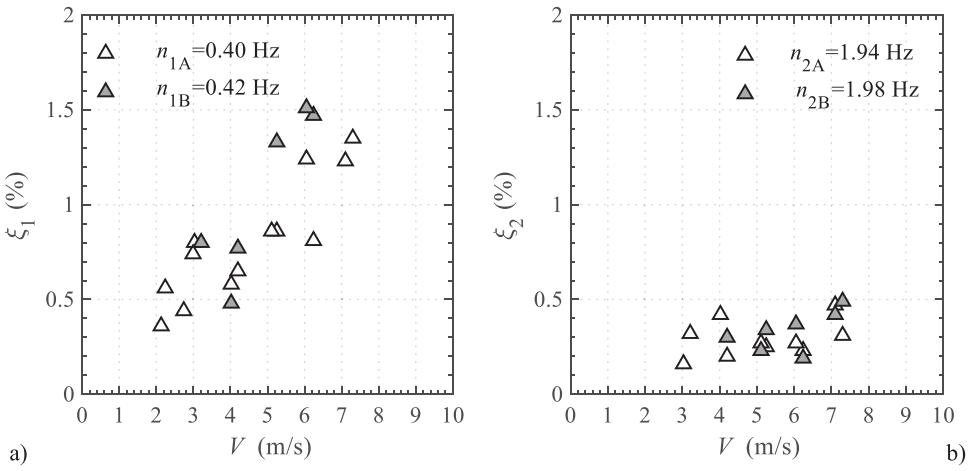

Fig. 11. First (a) and second (b) modal damping ratio versus mean wind speed of the lighting pole in Genova.

Table 2
Collected monopoles and main characteristics.

description (ref)	Shaft	height H (m), diameter ϕ and thickness t (mm)	equipment	modal frequency (Hz)	low displacement damping ratio (%)
lightning rod (this paper)	tapered 3 sections 16 sided	H= 30 ϕ_b= 770 (bottom) ϕ_t= 240 (top), t = 5	None	n_1= 0.87 n_2= 3.60	ξ_1= 0.17 ξ_2= 0.08 (pull and release)
lighting pole in La Spezia (this paper)	tapered 2 sections 16 sided	H= 16.6 ϕ_b = 530 (base) ϕ_t= 250 (top), t = 5	ladder, platforms, luminaire	n_1= 0.74, 0.84 n_2= 3.62, 3.93	ξ_1= 0.2 ξ_2= 0.7 (ambient)
high mast lighting pole in Genova (this paper)	tapered 4 sections 16 sided	H= 35 ϕ_b= 730 (base) ϕ_t= 770 (top), t = 8 (base); t = 8 (top)	light fixture	n_1= 0.39, 0.43 n_2= 1.94, 1.98	ξ_1= 0.45 ξ_2= 0.3 (ambient)
high mast lighting pole - Geo Tower [48]	tapered 3 sections 12 sided	H= 30 ϕ_b= 560 (base) ϕ_t= 200 (top), t = 10	light fixture and a lowering device	n_1= 0.33 n_2= 1.95	ξ_1= 0.65 ξ_2= 0.9 pull and release
street lighting pole [48]	tapered single piece circular	H= 12 ϕ_b= 188 (base) ϕ_t= 60 (top), t = 4	lamp	n_1= 1.15 n_2= 4.7	ξ_1= 0.24 ξ_2= 0.63 pull and release
street lighting pole [48]	5 sections stepped circular	H= 10 ϕ_b= 127 (base) ϕ_t= 60 (top), t = 3	lamp	n_1= 1.7 n_2= 4.7	ξ_1= 0.35 ξ_2= 0.62 pull and release
urban lighting pole [48]	5 sections tapered 8 sided	H= 14 ϕ_b= 280 (base) ϕ_t= 80 (top), t = 4	light fixture	n_1= 1.57	ξ_1= 0.55 eccentric mass vibrator
aluminum light pole [12]	tapered circular	H= 13.7 ϕ_b= 254 (base) ϕ_t= 152 (top), t = 5	lamp	n_1= 1.16	ξ_1= 0.1 (pull and release)
aluminum light pole [76]	tapered circular	H= 10.6 ϕ_b= 254 (base) ϕ_t= 152 (top), t = 5	a cantilever arm and lamp	n_1= 1.13	ξ_1= 0.18 (pull and release)
Two viaduct ligh poles, P1 and P2 [60]	tapered	H= 9.1 ϕ_b= 139.8 (base) ϕ_t= 89.1 (top), t = 5.7	lamp and signboard	n_1= 1.6 (P1) n_1= 1.56 (P2) n_2= 3.66 (P2)	ξ_1= 0.44 ξ_1= 0.55 ξ_2= 0.89 (ambient)
parked VAWT [44]	2 sections tapered 16 sided	H= 10.8 ϕ_b= 280 (base) ϕ_t= 80 (top), t = 4	Darrieus rotor	n_1= 1.49	ξ_1= 0.11 (ambient)
telecom monopole [28,29]	tapered	H= 14.5 n.a.	antennas, ladder, cables	n_1= 1.55	ξ_1= 0.55 (pull and release)

implemented to ensure clarity in the figures. Test number 2 is selected for the lightning rod due to its minimal dispersion. The data from Pagnini and Solari [48] are averaged over appropriately selected displacement amplitude intervals. The values from Jimenez Capilla et al. [28], originally presented in terms of structural acceleration, are converted into displacement amplitudes, derived approximately from the corresponding fundamental frequency. Straight lines in the figures represent estimates provided by codes. Eurocode [22] specifies a structural damping ratio of 0.2 % for the fundamental mode of uninsulated, unlined welded steel stacks. AASHTO [1] recommends 0.5 % for cantilevered signs and light supports, specifically suggesting, citing the NCHRP Report 464 [19], which notes that this value may not be conservative for light poles. Since specific values are generally not assigned for the second mode, technical assessments often adopt those specified

Fig. 12. 30-m Go Tower (a), 10-m stepped (b), 14-m street furniture (c).

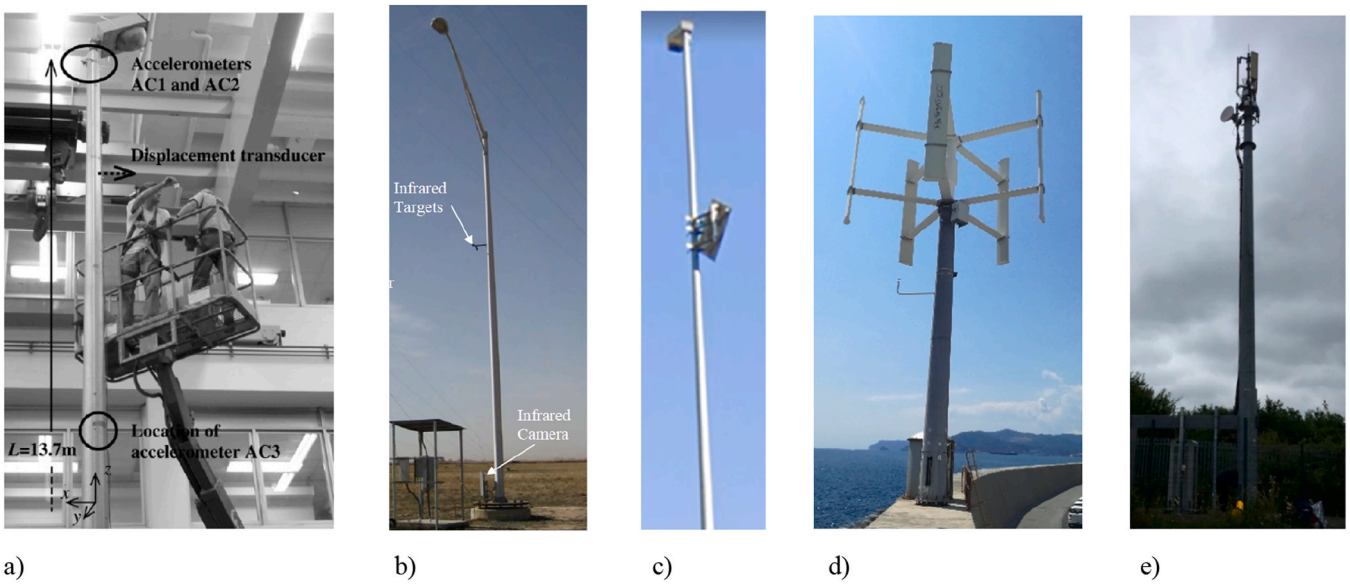

Fig. 13. Poles tested by (a) Caracoglia and Jones [12], (b) Zuo and Letchford [76], (c) Siringoringo et al. [60], (d) Pagnini, Piccardo [44], (e) Jimenez Capilla et al. [28,29].

for the first mode. The aerodynamic contribution, ξ_a, is expressed by:

$$\xi_a = \frac{c_F \rho \phi \ V}{4\pi n_1 m_e} \tag{3}$$

c_F being the force coefficient in the wind direction, ρ the air density, ϕ and V the diameter and the wind velocity at a representative structural height, m_e the equivalent mass per unit length.

Fig. 14a and Fig. 15a show the first and second modal damping ratios, respectively, as a function of wind velocity. Damping ratio estimated by the Eurocode is calculated as the sum of the mechanical and aerodynamic contribution. Although Eq. (3) does not account for luminaires and other equipment, it still appears to accurately capture the damping behaviour as a function of wind speed, thereby confirming the validity of the quasi-steady theory upon which the formulation is based.

Fig. 14b-c report the first modal damping ratios versus the top vibration amplitude related to the first mode, d_1. Fig. 15b report the second modal damping ratios as a function of the vibration amplitude, d_2 related to the second mode, measured at the level of the lower antinode. The comprehensive overview in Table 2 highlights the collected data and serves as a supplemental reference to Fig. 14 and Fig. 15.

Although the collected values exhibit heterogeneity, discernible trends can be observed. Damping ratios of the first mode at low vibration amplitude and wind speed are rather small. They are decidedly smaller for steel light poles without ladder or ancillaries (blue symbols in Fig. 14), ranging between 0.2 % and 0.35 %. These values increase rapidly with motion amplitude but then stabilize at levels not exceeding 0.5 %. The value suggested by the Eurocode appears generally suitable for conducting reasonably conservative analyses. Special attention should be given to the very low structural damping of bare and lightweight structures, such as the lightning rod and the two aluminum poles, which falls below 0.2 %. On the contrary, steel monopoles equipped with ancillaries and large light fixtures (black symbols in Fig. 14) exhibit damping values tendentially higher, ranging between 0.45 % and 0.65 %, therefore more in agreement with what provided by AASHTO for highway signs, luminaires, and traffic signals. The increasing trend in damping with motion amplitude seems pronounced, likely due to

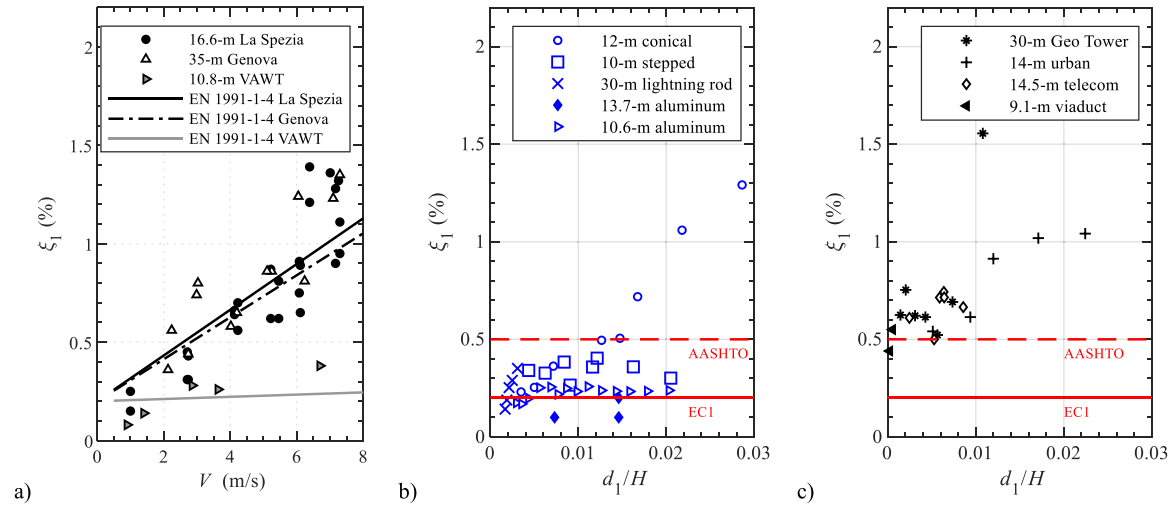

Fig. 14. Damping ratio of the first vibration mode versus: (a) wind velocity, (b) displacement at top for poles free of ancillaries, (c) displacement at top for poles with ancillaries and equipment.

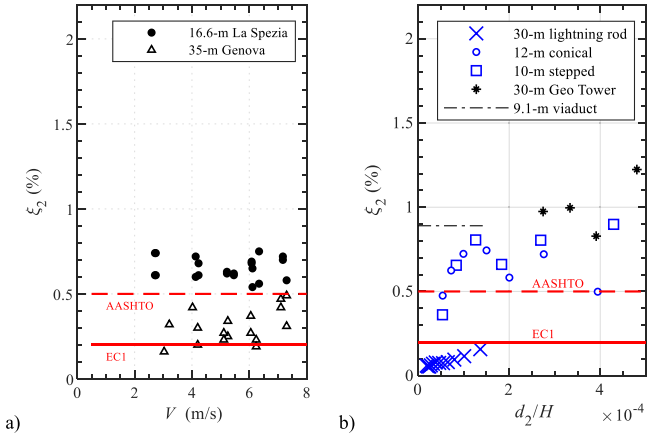

Fig. 15. Damping ratio of the second vibration mode versus: wind velocity (a) and displacement of the antinode (b) for poles free of ancillaries (blue symbols) and with ancillaries and equipment (black symbols).

friction from non-structural components and an enhanced aerodynamic contribution. As a result, a higher value can be used for gust-excited response. In this case, however, the additional aerodynamic contribution greatly reduces the relative importance of structural damping. Unlike what is observed for other types of structures [64], the variation with the amplitude of motion does not highlight a critical tip drift ratio, where the damping increasing tendency ends, at least in the amplitude range investigated in Fig. 14c.

Regarding the highlighted trends, there is some conflicting evidence: the damping of the 12 m conical pole deviates significantly from the overall pattern, displaying a sharply pronounced with motion amplitude. It has been included for completeness, but the authors believe these values are not suitable for deriving damping estimates. The 16.6-m La Spezia tower, despite having stairs, platforms, and multiple lights, exhibits quite low damping at low wind speeds. A similar behavior is observed for the wind turbine.

The diagrams for the damping ratio of the second mode show even greater variability. While the values are generally higher than those of the first mode, they are significantly lower in the case of the lightning rod. The damping of poles equipped with ancillaries tends to be higher overall. However, with the data currently available, it does not appear feasible to establish the same categorization or trends observed for the first method. Furthermore, the aerodynamic contribution seems minimal. In this context, the value recommended by Eurocode remains conservative but still inadequate for addressing bare poles effectively.

The third mode has been explored only to a limited extent in this investigation. Considering the findings reported in Section 3 from ambient tests, and from other studies in the literature, e.g., Ahearn and Puckett [2], Connor and Hodgson [17], the damping ratio of the third mode aligns with that of the second mode, but it is typically lower than the damping ratio of the first mode.

8. Conclusions

This paper discusses modal damping estimates for steel monotubular poles based on full-scale tests. It introduces new experiments for the dynamic identification of a lightning rod and two light poles, and offers a comprehensive collection of data from the scientific literature specifically focused on monotubular structures. The discussion of the ensemble values includes considerations on the international code prescriptions, aiming to provide valuable information for technical applications, such as addressing gust buffeting response, vortex-induced vibrations and fatigue issues. Special attention is given to the second vibration mode, which remain largely unexplored in the literature and for which no specifications are provided by current codes or guidelines. The main conclusions can be summarized as follows.

- The damping ratio of the first mode is generally low at small displacement amplitudes. For VIV and fatigue analysis, an average value of about 0.15 % is recommended for bare and lightweight poles, which is below the value suggested by Eurocode. Steel monopoles equipped with ancillary components typically exhibit higher damping values, though with significant variability, ranging from 0.2 % to 0.6 %. For these structures, a conservative estimate of 0.2 % is advisable.
- The damping ratio of bare and lightweight poles does not show a marked and uniform increase with the amplitude of motion and stabilizes at levels not exceeding 0.5 %. A typical value can be conservatively set at 0.3 % for gust buffeting analysis. In contrast, for structures with ancillary elements, damping exhibits a more consistent increase and continues to grow, at least within the considered range of amplitudes, and can be conservatively set at 0.5 %.
- The aerodynamic contribution to the gust-excited response is remarkably significant compared to the mechanical contribution. For the scenario analyzed, it appears to be well-represented by a quasi-steady approach employing the force coefficients recommended by the codes.

- The damping ratio of the second mode exhibits significant variability. Based on the available data, it is not currently possible to clearly differentiate between the various typologies, making it reasonable to adopt the standard value of 0.2 %. However, the extremely low value of the lightning rod stands out, therefore a conservative value of 0.1 % is recommended for bare structures, emphasizing the need to assess potential vortex shedding effects in this mode. Regarding gust buffeting response, the aerodynamic contribution is minimal and can generally be considered negligible for practical evaluations making the second mode potentially capable of contributing to the gust-induced response.
- The third mode is rarely significant in structural assessments. From the results obtained, it can be assumed in line with the second mode's characteristics.
- A summary table of catalogued values is provided to assist in estimating the damping for various types of poles. Defining variability ranges for damping ratios can enhance probabilistic assessments of wind vulnerability for slender monopole steel structures, leading to improved design and maintenance strategies.

CRediT authorship contribution statement

Luisa Carlotta Pagnini: Writing – review & editing, Writing – original draft, Validation, Methodology, Investigation, Data curation, Conceptualization. **Andrea Orlando:** Writing – review & editing, Validation, Investigation, Data curation. **Maria Pia Repetto:** Writing – review & editing, Methodology, Funding acquisition, Conceptualization.

Declaration of Competing Interest

The authors declare the following financial interests/personal relationships which may be considered as potential competing interests. Andrea Orlando, Maria Pia Repetto reports financial support was provided by European Union - NextGenerationEU and by the Ministry of University and Research (MUR). If there are other authors, they declare that they have no known competing financial interests or personal relationships that could have appeared to influence the work reported in this paper.

Acknowledgements

The Authors gratefully acknowledge the Laboratory of Geotechnical and Building Materials of the Genova University, the CTE SPA organization (Alessandria, Italy) and its Technical Director eng. Massimiliano Tassistro for the invaluable support and assistance throughout the tests. The second and third authors acknowledge the support by the European Union - NextGenerationEU and by the Italian Ministry of University and Research (MUR), National Recovery and Resilience Plan (NRRP), Mission 4, Component 2, Investment 1.5, Project "RAISE - Robotics and AI for Socio-economic Empowerment" (ECS00000035).

Data availability

Data will be made available on request.

References

[1] AASHTO. Standard Specifications for Structural Supports for Highway Signs, Luminaires, and Traffic Signals. 6th Edition. Washington D.C: American Association of State Highway and Transportation Officials; 2013.
[2] Ahearn E.B., Puckett J. (2010). Reduction of wind-induced vibrations in high-mast light poles. Report FHWA-WY-10/02F.
[3] Alexander LA, Wood J. A study of low-cycle fatigue failure of a galvanized steel lighting column. Eng Fail Anal 2009;16:2153–62.
[4] Au SK. Fast Bayesian FFT method for ambient modal identification with separated modes. J Eng Mech 2011;137(3):214–26.
[5] Au S.K. (2017). Operational Modal Analysis, Modeling, Bayesian Inference, Uncertainty Laws, Springer Singapore.
[6] Berntsen J, Brandt A, Gryllias K. Enhanced demodulation band selection based on Operational Modal Analysis (OMA) for bearing diagnostics. Mech Syst Signal Process 2024;181:109300.
[7] Brownjohn JMW, Magalhaes F, Caetano E, Cunha A. Ambient vibration re-testing and operational modal analysis of the Humber Bridge. Eng Struct 2010;32:2003–18.
[8] Brincker R, Ventura C. Introduction to Operational Modal Analysis. UK: John Wiley & Sons; 2015.
[9] Brincker R, Zhang L, Andersen P. Modal identification of output-only systems using frequency domain decomposition. Smart Mater Struct 2001;10:441–5.
[10] Burlando M, Zhang S, Solari G. Monitoring, cataloguing, and weather scenarios of thunderstorm outflows in the northern Mediterranean. Nat Hazards Earth Syst Sci 2018;18(9):2309–30.
[11] Calotescu I., Bitca D., Repetto M.P. (2021). Full-scale Behaviour of a Telecommunication Lattice Tower under Wind Loading. Lightweight Structures in Civil Engineering. Contemporary Problems. Proceedings of XVII International Seminar of IASS Polish.
[12] Caracoglia L, Jones NP. Numerical and experimental study of vibration mitigation for highway light poles. Eng Struct 2007;29:821–31.
[13] Chang B, Phares B, Sarkar P, Wipf T. Development of a procedure for fatigue design of slender support structures subjected to wind-induced vibration. Transp Res Rec J Transp Res Board 2009;2131:23–33.
[14] Chen GW, Omenzetter P, Beskhyroun S. Operational modal analysis of an eleven-span concrete bridge subjected to weak ambient excitations. Eng Struct 2017;151:839–60.
[15] Chen Y, Wang X, Sun C, Zhu B. Exploring the failure mechanism of light poles on elevated bridges under high winds. Eng Fail Anal 2024;159:108076.
[16] CNR (2010), Guide for the Assessment of Wind Actions and Effects on Structures – CNR-DT 207/2008, National Research Council of Italy, Rome.
[17] Connor R.J., Hodgson I.C. (2006). Field Instrumentation and Testing of High-Mast Lighting Towers in the State of Iowa. Final Report, Iowa Department of Transportation, Ames.
[18] Das G, Chakrabarty S, Dutta AK, Gupta KK, Ghosh RN. Failure analysis of a high mast lamp post. Eng Fail Anal 2006;13(7):1153–8.
[19] Dexter R.J., Ricker M.J. (2002). Fatigue-Resistant Design of Cantilevered Signal, Sign, and Light Supports. National Cooperative Highway Research Program, Report 469, Washington D.C.
[20] Dederichs AC, Øiseth O. Experimental comparison of automatic operational modal analysis algorithms for application to long-span road bridges. Mech Syst Signal Process 2023;199:110485.
[21] Dong X, Wang H, Guo K, Liu W, Zhao M. Field measurement and analysis on wind-induced vibration response of single column lighting rod. IET Conf Proc 2021:1744–50.
[22] EN 1991-1-4. Eurocode 1: Actions on Structures – Part 1.4: General Actions – Wind Actions. CEN. Brussels, Belgium: European Committee for Standardization; 2005.
[23] EN 1993-3-1. Eurocode 3: Design of steel structures - Part 3-1: Towers, masts and chimneys – Towers and masts. CEN. Brussels, Belgium: European Committee for Standardization; 2006.
[24] Ewins DJ. Modal Testing: Theory, Practice and Application. John Wiley & Sons Inc; 2000.
[25] García KL, Maes K, Parn VE, Lombaert G. Operational modal analysis of a self-supporting antenna mast. J Wind Eng Ind Aerodyn 2021;209:104490.
[26] Han Y, Zhou X, Wang L, Cai CS, Yan H, Hu P. Experimental investigation of the vortex-induced vibration of tapered light poles. J Wind Eng Ind Aerodyn 2021;211:104555.
[27] Jacobsen N.-J., Andersen P., Brincker R. (2008). Applications of Frequency Domain Curve-fitting in the EFDD Technique IMAC-XXVI: A Conference & Exposition on Structural Dynamics.
[28] Jimenez Capilla JA, Au S-K, Brownjohn JMW, Hudson E. Ambient vibration testing and operational modal analysis of monopole telecoms structures. J Civ Struct Health Monit 2021;11:1077–91.
[29] Jimenez Capilla JA, Wang Y, Brownjohn JMW. Damping estimation using free decays response in short telecom structures. Adv Struct Eng 2022;25(1):212–28.
[30] Liao Y, Wells V. Modal parameter identification using the log decrement method and band-pass filters. J Sound Vib 2011;330(21):5014–23.
[31] Magalhães F, Cunha Á, Caetano E, Brincker R. Damping estimation using free decays and ambient vibration tests. Mech Syst Signal Process 2010;24(5):1274–90.
[32] Matlab. Release 2018b, The MathWorks, Inc., Natick, Massachusetts, United States.
[33] Mengistu MT, Orlando A, Repetto MP. Wind and structural response monitoring of a lighting pole for the study of downburst effects on structures. J Wind Eng Ind Aerodyn 2023;240:105447.
[34] Mengistu MT, Repetto M. Dynamic response of a slender structure to thunderstorm outflow excitation through numerical analysis and full-scale monitoring. J Wind Eng Ind Aerodyn 2023;242:105556.
[35] Ni Y, Lu X, Lu W. Operational modal analysis of a high-rise multi-function building with dampers by a Bayesian approach. Mech Syst Signal Pr 2017;86:286–307.
[36] Orlando A. (2021). Full-scale Monitoring of the Wind-Induced Response of Vertical Slender Structures, with Fixed and Rotating Masses (Ph.D. thesis). University of Genoa.
[37] Orlando A, Pagnini L, Repetto MP. Structural response and fatigue assessment of a small vertical axis wind turbine under stationary and non-stationary excitation. Renew Energ 2021;170:251–66.
[38] Orlando A., Zerbino M. (2024). Compressive Sensing for Operational Modal Analysis of a prestressed concrete bridge. IOMAC 2024; Naples.

[39] Pagnini L. Model reliability and propagation of frequency and damping uncertainties in the dynamic alongwind response of structures. J Wind Eng Ind Aerodyn 1996;59(2,3):211–31.
[40] Pagnini L. Reliability analysis of wind excited structures. J Wind Eng Ind Aerodyn 2010;98:1–9.
[41] Pagnini L. A numerical approach for the evaluation of wind-induced effects on inclined, slender structural elements. Eur J Environ Civ Eng 2017;21(7–8):854–73.
[42] Pagnini LC, Burlando M, Repetto MP. Experimental power curve of small-size wind turbines in turbulent urban environment. Appl Energy 2015;154:112–21.
[43] Pagnini L, Piccardo G. A generalized gust factor technique for evaluating the wind–induced response of aeroelastic structures sensitive to vortex-induced vibrations. J Fluid Struct 2017;70:181–200.
[44] Pagnini L, Piccardo G. Modal properties of a vertical axis wind turbine in operating and parked conditions. Eng Struct 2021;242:112587.
[45] Pagnini L, Piccardo G, Repetto MP. Full scale behavior of a small size vertical axis wind turbine. Renew Energ 2018;127:41–55.
[46] Pagnini L, Piccardo G, Solari G. VIV regimes and simplified solutions by the spectral model description. J Wind Eng Ind Aerodyn 2020;198:104100.
[47] Pagnini LC, Repetto MP. The role of parameter uncertainties in the damage prediction of the alongwind-induced fatigue. J Wind Eng Ind Aerodyn 2012; 104–106:227–38.
[48] Pagnini L, Solari G. Damping measurements of steel poles and tubular towers. Eng Struct 2001;23:1085–95.
[49] Païdouissis MP, Price SJ, de Langre E. Fluid–Structure Interactions—Cross-Flow Induced Instabilities. New York: Cambridge University Press; 2011.
[50] Peeters B, De Roeck G. Reference-based stochastic subspace identification for output-only modal analysis. Mech Syst Signal Process 1999;13(6):855–78.
[51] Peeters B, De Roeck G. Stochastic system identification for operational modal analysis: a review. J Dyn Syst Meas Contr 2001;123(4):659–67.
[52] Pimenta F, Ribeiro D, Román A, Magalhães F. Modal properties of floating wind turbines. Anal Study Oper modal Anal Util-Scale Wind Turbine 2024;301:117367.
[53] Rainieri C, Fabbrocino G. Operational Modal Analysis of Civil Engineering Structures: An Introduction and Guide for Applications. Springer; 2014.
[54] Repetto MP, Solari G. Bimodal alongwind fatigue of structures. J Struct Eng 2006; 132(6):899–908.
[55] Repetto MP, Solari G. Closed form solution of the alongwind-induced fatigue damage to structures. Eng Struct 2009;31:2414–25.
[56] Repetto MP, Solari G. Wind-induced fatigue collapse of real slender structures. Eng Struct 2010;32:3888–98.
[57] Reynders E. System identification methods for (operational) modal analysis: review and comparison. Arch Comput Methods 2012;19(1):51–124.
[58] Reynders E., Schevenels M., De Roeck G. (2021). Macec 3.4. The Matlab toolbox for experimental and operational modal analysis. Report BWM-2021-04 <⟨http://bwk.kuleuven.be/bwm/macec/⟩> .
[59] Sarlo R, Tarazaga PA, Kasarda ME. High resolution operational modal analysis on a five-story smart building under wind and human induced excitation. Eng Struct 2018;176:279–92.
[60] Siringoringo DM, Wangchuk S, Fujino Y. Noncontact operational modal analysis of light poles by vision-based motion-magnification method. Eng Struct 2021;244: 112728.
[61] Solari G, Burlando M, Repetto MP. Detection, simulation, modelling and loading of thunderstorm outflows to design wind-safer and cost-efficient structures. J Wind Eng Ind Aerodyn 2020;200:104142.
[62] Solari G, Pagnini LC. Gust buffeting and aeroelastic behaviour of poles and monotubular towers. J Fluid Struct 1999;13(7-8):877–905.
[63] Solari G, Repetto MP, Burlando M, Tizzi M, Parodi M. The wind forecast for safety management of port areas. J Wind Eng Ind Aerodyn 2012;104–106:266–77.
[64] Tamura Y. Amplitude dependency of damping in buildings and critical tip drift ratio. Int J High-Rise Build 2012;1:1–13.
[65] Tamura Y. Damping in Buildings and Estimation Techniques. In: Tamura Y, Kareem A, editors. Advanced Structural Wind Engineering. Tokyo: Springer; 2013.
[66] Taplin G., Sanders G., Maklary Z. (2006). Fatigue Failures of Light Poles. In Proceedings of the Austroads 6th Bridge Conference: Bridging the Gap, Perth, Australia.
[67] Tranvik P., Alpsten G. (2002). Dynamic Behaviour under Wind Loading of a 90 m Steel Chimney, Report S-01041.
[68] Verboom GK, van Koten H. Vortex excitation: three design rules tested on 13 industrial chimneys. J Wind Eng Ind Aerodyn 2010;98:145–54.
[69] Vickery BJ, Basu RI. Across-wind vibrations of structures of circular cross-section. Part I: development of a mathematical model for two-dimensional conditions. J Wind Eng Ind Aerodyn 1983;12(1):49–74.
[70] Xhelaj A, Orlando A, Pagnini L, Tubino F, Repetto M. Fatigue life assessment of a slender lightning rod due to wind excited vibrations. Procedia Struct Integr 2024; 57:754–61.
[71] Yam LH, Leung TP, Li DB, Xue KZ. Use of ambient response measurements to determine dynamic characteristics of slender structures. Eng Struct 1997;19(2): 145–52.
[72] Ye J, Niu H, Yang F, Huang G, Chen Z. Experimental investigation of wind-induced vibration of multi-cross-section steel tube lightning rods in substation. J Wind Eng Ind Aerodyn 2024;253:105863.
[73] Zhang M, Li T, Wang Y, Chen Y, Zhao G. Wind-induced vibration and vibration suppression of high-mast light poles with spiral helical strakes. Buildings 2023;13: 907.
[74] Zhao G, Li J, Zhang M, Yi Y. Experimental study on the bearing capacity and fatigue life of lightning rod structure joints in high-voltage substation structures. Thin-Walled Struct 2022;175:109282.
[75] Zou L, Qiu F, Xu G, Shi T, Kareem A. Contribution of the second mode to wind-induced response of prismatic tall buildings. Eng Struct 2025;322:119202.
[76] Zuo D., Letchford C. (2008). Investigation of Wind-Induced Highway Lighting Pole Vibration Using Full-Scale Measurement. Report FHWA/TX-08/0-4586-5.